Polyoxometalates RESEARCH ARTICLE

Effect of protons on the structure and catalytic oxidation performance of Zr-substituted Wells-Dawson phosphotungstates

Sofia M. Marikovskaya [1], Nataliya V. Maksimchuk [1], Olga V. Zalomaeva [1], Vasilii Yu. Evtushok [1], Artem A. Antonov [1], Jordi Puiggalí-Jou [2], Albert Solé-Daura [2,3], Vadim V. Yanshole [4], Jorge J. Carbó [2] ✉, and Oxana A. Kholdeeva [1] ✉

[1] *Boreskov Institute of Catalysis, Novosibirsk 630090, Russia*
[2] *Universitat Rovira i Virgili, Departament de Química Física i Inorgànica, 43007 Tarragona, Spain*
[3] *Institute of Chemical Research of Catalonia (ICIQ-CERCA), The Barcelona Institute of Science and Technology, 43007 Tarragona, Spain*
[4] *International Tomography Center SB RAS, Novosibirsk 630090, Russia*

Received: 26 June 2026; **Revised:** 26 October 2026; **Accepted:** 1 November 2026

✉Address correspondence to Jorge J. Carbó, j.carbo@urv.cat; Oxana A. Kholdeeva, khold@catalysis.ru

Cite This: *Polyoxometalates*, 2027, *6*, 9140172 Read Online

ABSTRACT: A series of tetra-*n*-butylammonium (TBA) salts of Zr-monosubstituted phosphotungstates of the Wells-Dawson structure (**Zr-D**) were prepared by varying pH in the range of 1.5–4.5 during the synthesis. The compounds were characterized by elemental analysis, TGA, potentiometric titration, FT-IR spectroscopy, ^{31}P NMR, and high-resolution ESI-MS. A combination of CHN analysis, thermogravimetry, and potentiometric titration with TBAOH point to different composition of the cationic sphere of **Zr-D**, namely the ratio of H^+/K^+, which increased with decreasing pH of the TBA salt precipitation. Spectroscopic studies (FT-IR, ^{31}P NMR, and ESI-MS) implicated that the polyanion state in the **Zr-D** samples depends on the acidity. While **Zr-D** obtained at pH 1.5–2.0 is a monomer, $TBA_{5.5}K_{0.5}[\alpha_2\text{-}P_2W_{17}O_{61}Zr(H_2O)_3]$, the samples prepared at pH 3.5–4.5 have a dimeric structure, $TBA_{11}K_3[\{P_2W_{17}O_{61}Zr(\mu\text{-}OH)\}_2]\cdot xH_2O$ (x = 7–8), in the solid state, with a tendency to monomerization in dilute acetonitrile solutions producing $[P_2W_{17}O_{61}Zr(\mu\text{-}OH)]^{7-}$. DFT simulations of the IR and NMR spectra show that the spectral changes originate from variations in the protonation state, hydration degree, and monomer–dimer speciation of the Zr-substituted Wells–Dawson polyanions. Catalytic properties of **Zr-D** were assessed in the oxidation of thioethers using H_2O_2 as oxidant. **Zr-D** prepared at pH 1.5–2.0 and containing terminal $Zr(H_2O)$ showed higher activity and sulfoxide yields than **Zr-D** with terminal Zr-OH prepared at higher pH values. A comparison of Zr-substituted polyoxotungstates of the Wells-Dawson, Keggin and Lindqvist structures revealed a correlation between catalytic activity and the polyanion charge density, which in turns modulates the local electronic environment of the Zr center.

KEYWORDS: hydrogen peroxide, polyoxometalate, zirconium, sulfoxidation, polyanion charge density, DFT

Just Accepted

1 Introduction

Over many years, zirconium-based compounds and materials were largely overlooked as viable catalysts for liquid-phase selective oxidations with H_2O_2, primarily because of their high propensity to undergo hydrolysis and polymerization, resulting in low Lewis acidity [1, 2]. Zr-silicates synthesized using different approaches showed notable activity in homolytic H_2O_2-based oxidations, while their applicability to heterolytic activation of H_2O_2 remained questionable [3–5]. Meanwhile, Zr-based metal-organic frameworks (Zr-MOFs), in particular those of the UiO family [6], have emerged as promising candidates for stable and recyclable oxidation catalysts [7–14]. This has led to a surge of scientific interest in the use of zirconium to activate H_2O_2 and, in particular, to intensified investigations on zirconium-substituted polyoxometalates (Zr-POMs) [15–20].

Over the years, POMs, which are anionic clusters composed of early transition metals and oxygen [21, 22], have captivated researchers across multiple disciplines, including materials science [23–29], medicine [30–33], and catalysis [24,29, 34–44] due to their unique and tunable composition, structures and reactivity. One of the compelling aspects of POMs is their structural similarity to metal oxide surfaces [45–48]. This allows polyoxometalates to be considered as valuable molecular models that can be investigated at the atomic level using both experimental and computational techniques to elucidate the mechanisms of selective oxidation catalysis [49–54].

Although numerous Zr-POMs have been reported in the literature [55,56], only a select few have been investigated for their potential in catalyzing oxidation reactions using H_2O_2. In 2006, Kholdeeva et al. synthesized tetra-*n*-butyl ammonium (TBA) salts of a Zr-monosubstituted Keggin-type dimer, [{α-

$PW_{11}O_{39}Zr(\mu\text{-}OH)\}_2]^{8-}$, with different protonation state and demonstrated that the protonated form $TBA_7H[\{\alpha\text{-}PW_{11}O_{39}Zr(\mu\text{-}OH)\}_2]$ is highly active in homolytic oxidations with H_2O_2 [57]. Kortz and co-workers have reported the first example of a Zr-POM, $[TBA_7H_4[Zr_6O_4(OH)_4(H_2O)_2(CH_3COO)_5(AsW_9O_{33})_2]$, capable of heterolytic activation of H_2O_2 and epoxidation of alkenes featuring highly reactive allylic hydrogen atoms [58]. Nomiya's group synthesized several Zr-POMs with distinct structural characteristics and evaluated their catalytic performance for the epoxidation of alkenes with H_2O_2 [59]. Among them, only $TBA_7H[\{\alpha\text{-}PW_{11}O_{39}Zr(\mu\text{-}OH)(H_2O)\}_2]\cdot 3H_2O$ combined noticeable catalytic activity in the epoxidation of *cis*-cyclooctene with structural stability under catalyst turnover conditions [59]. The authors suggested binding of both C=C bond and hydroperoxo moiety to Zr site. An isolated bridged di-peroxo complex, $(Et_2NH_2)_{10}[\{Zr(\mu\text{-}\eta^2\text{-}O_2)\}_2(\alpha\text{-}PW_{11}O_{39})_2]$, was almost inert.

Further contributions to the investigation of POM-embedded Zr peroxides were made by Kortz and co-workers, who reported synthesis, characterization and reactivity of Keggin POM-based peroxo complexes, $[Zr_6(O_2)_6(OH)_6(\gamma\text{-}SiW_{10}O_{36})_3]^{18-}$ [60,61] and $[Zr_2(O_2)_2(XW_{11}O_{39})_2]^{12-}$ (X = Si or Ge) [61, 62]. These compounds exhibited activity in both stoichiometric [61,62] and catalytic [61] oxidation of L-methionine in aqueous media and also demonstrated their potential as catalysts in oxidizing alcohols with H_2O_2 in biphasic systems [61].

Recently, Walls et al. have synthesized a Zr(IV)-substituted polyoxovanadate, $TBA[ZrV_5O_6(OCH_3)_{13}]$ (**ZrV$_5$**), and demonstrated its high selectivity toward the formation of sulfoxides in catalytic oxidations with H_2O_2-urea [63]. A **ZrV$_5$**-derived terminal peroxide was inactive toward thioethers under stoichiometric conditions. A range of Zr-containing POMs have been prepared and tested for the oxidation of thioethers with excess of H_2O_2, producing sulfones [64–71].

The exploration of Zr-POMs in oxidation catalysis continues to be a promising area of research, with ongoing studies aimed at understanding the mechanisms of their catalytic action, optimizing their composition and structures for enhancing activity and selectivity, and expanding their applications in organic synthesis and environmental chemistry.

Our research interest in Zr-POMs was heightened by the recent discovery that Zr-monosubstituted Lindqvist-type dimer $TBA_6[\{W_5O_{18}Zr(\mu\text{-}OH)\}_2]$ (**Zr-L**) is able to heterolytically activate H_2O_2 and accomplish a range of selective oxidations, including thioether sulfoxidation and epoxidation of alkenes and α,β-unsaturated ketones [15]. Experimental studies and DFT calculations on the interaction of **Zr-L** with H_2O_2 revealed the formation of both dimeric and monomeric Zr peroxo species capable of electrophilic oxygen atom transfer to thioethers ($[(\mu\text{-}\eta^2\text{:}\eta^2\text{-}O_2)\{ZrW_5O_{18}\}_2]^{6-}$ and $[W_5O_{18}Zr(\eta^2\text{-}OOH)]^{3-}$) and C=C bonds ($[W_5O_{18}Zr(\eta^2\text{-}OOH)]^{3-}$ only) [15]. We also found that **Zr-L** generates singlet oxygen during decomposition of H_2O_2, resulting in an ene-type reactivity [16]. Computational studies inferred the formation of a Zr-trioxidane {Zr-η^2-OO(OH)} key intermediate upon interaction of the Zr peroxo species with a second H_2O_2 molecule [16].

In 2023, we revisited our early results on H_2O_2-based oxidations in the presence of Zr-POMs of the Keggin structure and found that dimer $TBA_8[\{PW_{11}O_{39}Zr(\mu\text{–}OH)(H_2O)\}_2]$ (**Zr-K**) can serve as efficient catalyst for epoxidation of various kinds of alkenes, including terminal ones [17]. Surprisingly, additives of acid and base produced opposite effects on the catalytic performance of **Zr-L** [15] and **Zr-K** [17]. In addition, **Zr-K** revealed unprecedentedly high activity in the oxidation of organic sulfides (the reaction was completed within seconds at room temperature) [18] but, in contrast to **Zr-L**, it did not show ene-type reactivity [16].

Such a significant and, at first glance, poorly understood difference in the catalytic performances of **Zr-L** and **Zr-K** prompted us to turn our attention to a Zr-monosubstituted phosphotungstate of the Wells-Dawson structure $[\{P_2W_{17}O_{61}Zr(\mu\text{-}OH)\}_2]^{14-}$ (**Zr-D**), which was first prepared and structurally characterized by Nomiya and co-workers [72]. So far, **Zr-D** and related compounds were extensively studied in acid–base catalysis [73–79], but their potential for oxidation catalysis remained underexplored. Kortz and co-workers have reported the synthesis and characterization of a di-peroxo dimer, $TBA_{10}H_5K[Zr_2(O_2)_2(P_2W_{17}O_{61})_2]$ (shortly, **Zr(O$_2$)-D**), and its Hf analogue, which showed no activity towards organic substrates under stoichiometric conditions but could act as catalyst for H_2O_2 activation and oxidation of some specific organic substrates via a homolytic mechanism [19]. However, catalytic performance of peroxo-free **Zr-D** was not investigated.

In the present work, we fill this gap with the aim to establish synthesis–composition–structure–activity relationships for **Zr-D** and to deepen our understanding of the factors governing Zr-POM reactivity in selective oxidations. To this end, a series of TBA-salts of **Zr-D** were synthesized, varying pH in the range of 1.5–4.5. The elaborated **Zr-D** samples were thoroughly characterized by experimental and computational methods and their catalytic performance was assessed in the oxidation of thioethers with H_2O_2 and compared with the catalytic performance of **Zr-K** and **Zr-L**. This study unveiled the effect of acidity during the synthesis on the composition, structure and catalytic properties of **Zr-D** and also helped us to rationalize the structural effect in the oxidation catalysis with Zr-POMs, where the crucial role of polyanion charge density was implicated.

2 Experimental

2.1. Synthesis and characterization of Zr-D

A series of TBA salts of Zr-monosubstituted Wells-Dawson POMs were prepared following a procedure described by Saku et al. with some modifications. Precipitation of the TBA salts was carried out at different pH values in the range of 1.5–4.5 (see Supporting Information (SI) for details), and the corresponding POM samples were designated as **Zr-D-X**, where X is the pH value. Samples of **Zr-D** were characterized by elemental analysis, thermogravimetry (TGA), potentiometric titration, FT-IR, ^{31}P NMR, and high-resolution electrospray

Just Accepted

ionization mass spectrometry (HR-ESI-MS). TGA measurements (Figure S1) performed in a He atmosphere showed a weight loss of 0.5-1.3% below 200 °C, consistent with the presence of 3–4 water molecules per Zr (most likely, solvated and/or adsorbed water from the atmosphere). Potentiometric titration data indicated a gradual decrease in the number of acidic protons in **Zr-D** samples upon increasing pH of their precipitation (Figure S2).

Zr-D-1.5 (precipitation at pH 1.5). Anal. Calc. for $TBA_{5.5}K_{0.5}[\alpha_2\text{-}P_2W_{17}O_{61}Zr(H_2O)_3]$ (%): C, 18.67; H, 3.59; N, 1.36. Found: C, 18.00; H, 3.50; N, 1.30. ^{31}P NMR (ppm, 0.01 M in CH_3CN + 5 vol% H_2O, 25 °C): δ −10.29 (s, 1 P, PW_8Zr), −12.68 (s, 1 P, PW_9). IR (cm^{-1}, KBr): 1150 w, 1091 s, 1020 w, 960 s, 909 s, 787 s, 742 sh, 598 w, 526 m.

Zr-D-2.0 (precipitation at pH 2.0). Anal. Calc. for $TBA_{5.5}K_{0.5}[\alpha_2\text{-}P_2W_{17}O_{61}Zr(H_2O)_3]$ (%): C, 18.67; H, 3.59; N, 1.36; Zr 1.61; W, 55.20; K, 0.35. Found: C, 18.40; H, 3.80; N, 1.10; Zr, 1.45; W, 55.80; K 0.20. ^{31}P NMR (ppm, 0.01 M in CH_3CN + 5 vol% H_2O, 25 °C): δ −10.35, −12.77. IR (cm^{-1}, KBr): 1150 w, 1091 s, 1017 w, 960 s, 909 s, 787 s, 742 sh, 598 w, 526 m.

Zr-D-2.5 (precipitation at pH 2.5). Anal. Calc. for $TBA_{5.5}K_{0.5}[\alpha_2\text{-}P_2W_{17}O_{61}Zr(H_2O)_3]$ (%): C, 18.67; H, 3.59; N, 1.36. Found: C, 18.63; H, 3.65; N, 1.15. ^{31}P NMR (ppm, 0.01 M in CH_3CN + 5 vol% H_2O, 25 °C): δ −10.28, −13.11. IR (cm^{-1}, KBr): 1151 w, 1089 s, 1014 w, 952 s, 909 s, 819 sh, 786 s, 755 sh, 656 w, 598 w, 525 m.

Zr-D-3.0 (precipitation at pH 3.0). Anal. Calc. for $TBA_{11}K_{2.5}H_{0.5}[\{P_2W_{17}O_{61}Zr(\mu\text{-}OH)\}_2]\cdot 8H_2O$ (%): C, 18.46; H, 3.65; N. 1.34; Zr 1.59; W, 54.58; K, 0.85. Found: C, 18.80; H, 3.62; N, 1.20; Zr, 1.50; W, 54.2; K, 0.55. ^{31}P NMR (ppm, 0.01 M in CH_3CN + 5 vol% H_2O, 25 °C): δ −10.29, −13.30. IR (cm^{-1}, KBr): 1153 w, 1089 s, 1014 w, 951 s, 910 s, 820 sh, 786 s, 753 sh, 660 w, 598 w, 525 m.

Zr-D-3.5 (precipitation at pH 3.5). Anal. Calc. for $TBA_{11}K_{2.5}H_{0.5}[\{P_2W_{17}O_{61}Zr(\mu\text{-}OH)\}_2]\cdot 8H_2O$ (%): C, 18.46; H, 3.65; N. 1.34. Found: C, 18.40; H, 3.80; N, 1.20. ^{31}P NMR (ppm, 0.01 M in CH_3CN + 5 vol% H_2O, 25 °C): δ −10.29, −13.35. IR (cm^{-1}, KBr): 1151 w, 1089 s, 1014 w, 949 s, 910 s, 816 sh, 786 s, 753 sh, 660 w, 598 w, 526 m.

Zr-D-4.0 (precipitation at pH 4.0). Anal. Calc. for $TBA_{11}K_3[\{P_2W_{17}O_{61}Zr(\mu\text{-}OH)\}_2]\cdot 7H_2O$ (%): C, 18.46; H, 3.62; N, 1.35; Zr 1.59; W, 54.57; K, 1.02. Found: C, 18.20; H, 3.70; N, 1.00; Zr, 1.53; W, 55.3; K, 0.68. ^{31}P NMR (ppm, 0.01 M in CH_3CN + 5 vol% H_2O, 25 °C): δ −10.28, −13.41. IR (cm^{-1}, KBr): 1152 w, 1088 s, 1015 w, 950 s, 911 s, 821 sh, 788 s, 755 sh, 660 w, 598 w, 5265 m.

Zr-D-4.5 (precipitation at pH 4.5). Anal. Calc. for $TBA_{11}K_3[\{P_2W_{17}O_{61}Zr(\mu\text{-}OH)\}_2]\cdot 8H_2O$ (%): C, 18,43; H, 3,63; N, 1.34. Found: C, 18.60; H, 3.60; N, 1.10. ^{31}P NMR (ppm, 0.01 M in CH_3CN + 5 vol% H_2O, 25 °C): δ −10.28, −13.41. IR (cm^{-1}, KBr disk): 1153 w, 1089 s, 1013 w, 950 s, 911 s, 821 sh, 786 s, 752 sh, 660 w, 598 w, 524m.

For the sake of comparison TBA salts of **Zr-K** and **Zr-L** were also synthesized following the procedures reported previously [15,17] (see SI for details).

2.2. Catalytic reactions and product analyses

Catalytic oxidations were performed under vigorous stirring (500 rpm) in thermostated glass vessels. Each experiment was reproduced 2–3 times. Reactions were started by the addition of H_2O_2 to the reaction mixture containing solvent, substrate, and Zr-POM. The oxidation products were identified by gas chromatography–mass spectrometry (GC-MS).

Typical reaction conditions for methyl phenyl sulfide (MPS) oxidation: MPS 0.1 M, H_2O_2 0.1 M, Zr 0.002 M, CH_3CN 1 mL, 27 °C. The amount of water introduced into the solution did not exceed 1 % v/v and did not affect the catalyst solubility; the reaction mixture was visually transparent. The product yields and MPS conversions were quantified by gas chromatography (GC) using biphenyl as an internal standard. In kinetic experiments, aliquots were rapidly withdrawn from the reaction mixture and treated with a solution of PPh_3 in order to decompose unreacted H_2O_2. Initial rates of MPS consumption were determined from the reaction profiles by linear approximation of the first 6–7 points of the kinetic curves at low conversions (<10%).

Typical reaction conditions for thianthrene-5-oxide (SSO) oxidation: SSO 0.025 M, H_2O_2 0.0038 M, Zr 0.0005 M, CH_3CN 2 mL, 27 °C. After 10 min, the reaction mixture was evaporated, the reaction products were dissolved in $CHCl_3$ while the insoluble catalyst was filtered off. $CHCl_3$ was replaced by deuterated $CDCl_3$ for ^{1}H NMR analysis of the product composition. SSO conversion and product yields were calculated from the ^{1}H NMR spectra by integration of corresponding signals [.80].

3 Results and discussion

3.1. Synthesis and characterization of Zr-D

According to the literature [55,72,77–79, 81–83], Zr-substituted Wells-Dawson-type POMs can exist in several forms: 2:2 dimer [72], 1:1 monomer [72,74,83], and 1:2 complex [72,81,82]. All these forms can convert to each other depending on the temperature, pH, concentration, and the presence of some substrates [72,78,79]. However, the information about specific conditions favorable for the formation of 2:2 dimer and 1:1 monomer remained so far contradictory. Nomiya and co-workers have reported the synthesis (at pH 2.0) and structural characterization of the 2:2 dimer $(Me_2NH_2)_{14}[\{\alpha_2\text{-}P_2W_{17}O_{61}Zr(\mu\text{-}OH)(H_2O)\}_2]\cdot 16H_2O$ [72]. However, subsequent ^{31}P NMR studies on aqueous solutions of this Zr-POM revealed that pH 3.5 is a 'breaking point' in the transformation of the 2:2 dimeric species to the monomeric ones [72]. While the 2:2 complex dominated at pH values > 4.0, the 1:1-type species were observed at pH 1.50–0.50 [72,79]. Sokolov et al. demonstrated that the 2:2 complex undergoes cleavage of the hydroxo bridges with the formation of the 1:1 complex $[(H_2O)_3Zr(P_2W_{17}O_{61})]^{6-}$ in 1–2 M HCl (pH values close to zero) [83]. To figure out how the synthesis conditions affect the state of **Zr-D** and its catalytic performance, we prepared a series of TBA salts by systematically varying pH in the range 1.5–4.5 before adding TBABr.

Just Accepted

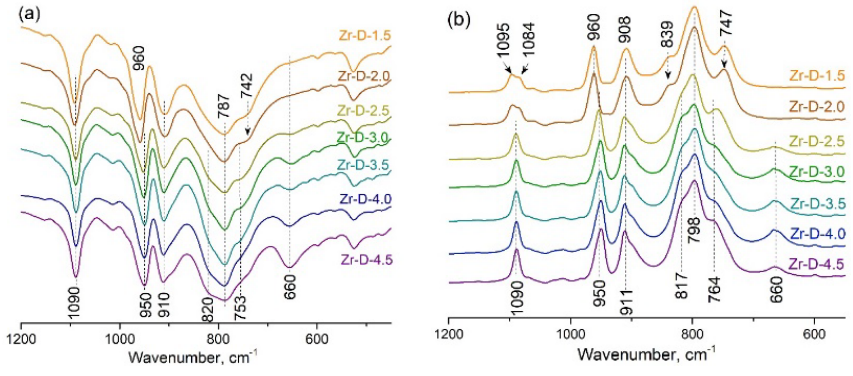


Figure 1 IR spectra of **Zr-D**: (a) in KBr pellets and (b) ATR-IR in dry acetonitrile (0.01 M solutions).

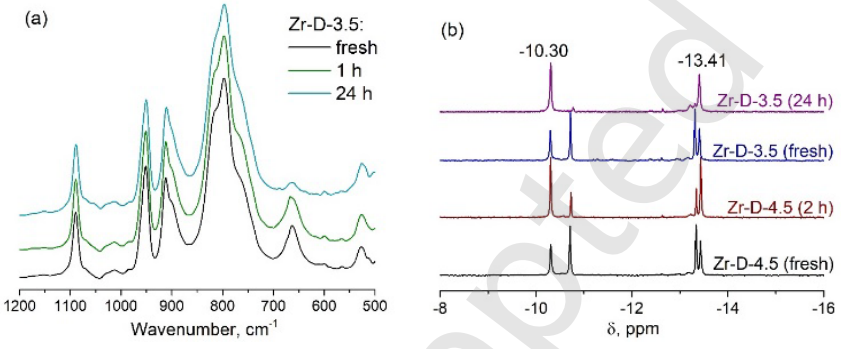


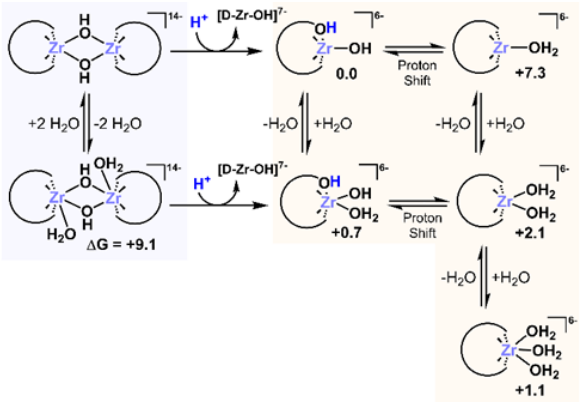
Figure 2 (a) ATR-FT-IR and (b) ^{31}P NMR spectra of **Zr-D** (0.01 M) prepared at pH 3.5 and 4.5 collected in dry CH_3CN: freshly prepared solutions and kept in air at room temperature.

FT-IR spectra of solid **Zr-D** in KBr and ATR-FT-IR spectra of their 0.01 M solutions in CH_3CN (Figure 1) look similar and are close to the IR spectra reported in the literature for Zr-substituted Wells-Dawson phosphotungstates [19,83]. The spectra exhibit the principal bands of the Wells-Dawson structure corresponding to the vibrations ν(P–O) at 1090 cm^{-1} (split in the ATR-IR spectra of **Zr-D-1.5** and **Zr-D-2.0**), ν(W=O) at 950 (samples precipitated at pH 3.0–4.5) or 960 cm^{-1} (**Zr-D-1.5** and **Zr-D-2.0**), and ν(W–O–W) at 908–911 and 798 cm^{-1}. In addition, all **Zr-D** display a shoulder, which is shifted from 839 cm^{-1} (**Zr-D-1.5** and **Zr-D-2.0**) to 817 cm^{-1} (other samples), most likely, corresponding to ν(Zr–O–W), and a band at 747 cm^{-1} (for **Zr-D-1.5** and **2.0**) or 764 cm^{-1} (samples precipitated at pH 3.0–4.5), which was previously assigned to ν(Zr–O(H)–Zr) vibrations [57, 84]. To summarize, the spectra of the **Zr-D** samples prepared at pH 3.0–4.5 are very close, while the spectra of **Zr-D-1.5** and **Zr-D-2.0** reveal some significant differences: the frequencies of ν(W=O) are shifted to higher energy (960 vs 950 cm^{-1}), reflecting a slight increase in terminal oxygen to Zr π-bonding upon protonation. On the contrary, a lower-energy shift is observed for ν(Zr–O(H)–Zr) on going from **Zr-D-4.5** to **Zr-D-1.5**, which can also reflect changes in the protonation state of the polyanion and/or alteration of its nuclearity.

The crucial role of acidity (polyanion protonation) in these transformations was confirmed by *in situ* ATR-FT-IR experiments respectively (Figure S3). As it was mentioned above, there is a splitting of the ν(P–O) vibration in the solution spectra of **Zr-D-1.5** and **Zr-D-2.0** (Figure 1b), which may be due to loss of symmetry upon monomerization of **Zr-D** with the formation of terminal $\{Zr(OH)_n(H_2O)_m\}$ (n + m = 3). This splitting disappears upon addition of 1 vol.% of water (Figure S4b), most likely, owing to acceleration of exchange processes. A band at 660 cm^{-1}, which is present in the IR spectra of **Zr-D** samples prepared at pH 2.5 and higher and missing for the samples **Zr-D-1.5** and **Zr-D-2.0,** disappears upon addition of acid or water to **Zr-D-4.0** (Figures S3a and S4a). However, this band does not appear upon addition of base to the sample **Zr-D-2.0** (Figure S3b). Moreover, it disappears simply upon storing of the acetonitrile solution of **Zr-D-3.5** at room temperature (Figure 2a).

Density functional theory (DFT) calculations [85] were performed to investigate the possible structures of the Zr-substituted Wells–Dawson species formed under different synthesis conditions. Distinct protonation and hydration patterns were explored for both monomeric and dimeric species, based on previous studies on Zr-substituted polyoxometalates [72,74,79,81, 86, 87, 88]. As compiled in Scheme 1, several dimeric and protonated monomeric species were found to lie within a narrow Gibbs free-energy range, indicating that multiple closely related species are likely to coexist in similar synthetic conditions. In particular, the speciation is expected to depend on both the presence or absence of coordinated water molecules at the Zr center and the location of the proton(s) forming hydroxo or aqua ligands. Note however that the complexity associated with an accurate estimation of the entropic contribution to hydration energies makes these values difficult to evaluate reliably, and they should therefore be interpreted with caution [86]. For instance, for the dimeric

Just Accepted



Scheme 1 Gibbs free-energy diagram of the predominant species of the synthesized **Zr-D** under different conditions. All the displayed energies are in kcal mol^{-1} and values in parenthesis are referred to the protonated hydroxo species.

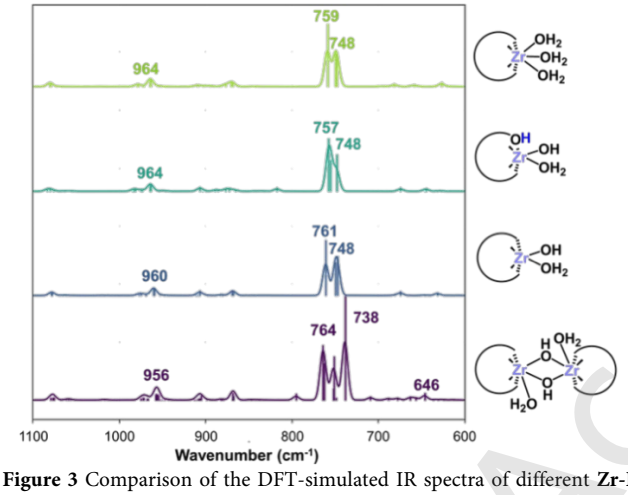


Figure 3 Comparison of the DFT-simulated IR spectra of different **Zr-D** dimeric and monomeric species containing aqua ligands. See Figure S5 for further details about band assignments and comparison with aqua ligand-free systems.

species, we estimate a Gibbs free-energy cost of +9.1 kcal mol^{-1} for the formation of the "hydrated" species $\{\alpha_2\text{-}P_2W_{17}O_{61}Zr(\mu\text{-}OH)(H_2O)\}_2$ from to the "anhydrous" one (see Scheme 1), but the hydration degree would depend on the local availability of water molecules. For protonated monomeric species, the hydroxo-aqua and the triaqua complexes are within 1 kcal·mol^{-1}.

The optimized structures were subsequently used to simulate IR spectra in order to identify the structural origin of the experimental spectral changes observed between samples synthesized at low and high pH (Figures 3 and S5). Two main trends emerge from the calculations. First, the computed spectra explain the approximately 10 cm^{-1} blue shift of the terminal W=O stretching band observed experimentally upon going from samples precipitated at pH 3.0-4.5 to pH 1.5-2.5. Starting at the dimeric, di-hydroxo bridged, species (ν(W=O) =956 cm^{-1}), the shift arises from two contributions at lower pH: monomerization with a computed band at 960 cm^{-1} for Zr-hydroxo-aqua species, and protonation that provides an addition blue shift to 964 cm^{-1} for protonated Zr-hydroxo-aqua and Zr-triaqua species. Second, the experimental band at 660 cm^{-1}, present only in the high-pH (dimeric) samples, is assigned to the out-of-plane bending mode of the bridging $Zr(OH)_2Zr$ unit. In the simulated spectra, this vibration appears at 646 cm^{-1} and coupled with rocking modes of Zr-OH_2 groups, explaining the array of features observed in this region. In contrast, this band is absent in the monomeric species, consistent with the experimental spectra of samples obtained at low pH. The calculations, however, do not provide a straightforward interpretation of the spectral region between 700 and 800 cm^{-1}, where many strongly coupled W–O–W and W–O–Zr vibrations give rise to a complex pattern of overlapping bands. Overall, the IR simulations further support that samples prepared at low pH correspond to monomeric species, while at pH 3.5-4.5 dimeric species are obtained.

Solutions of **Zr-D** in CH_3CN were then investigated by ^{31}P NMR spectroscopy to verify the suggestions made on the basis of the analysis and DFT simulations of the IR spectra. Note that comparison of the ^{31}P NMR spectra obtained in this work with those reported in the literature is problematic since, in previous works, ^{31}P NMR spectra were almost exclusively collected in H_2O/D_2O or DMSO solutions for Me_2NH_2 salts of **Zr-D** [72,83]. In D_2O, the spectrum of the 2:2-type complex $(Me_2NH_2)_{14}[\{\alpha_2\text{-}P_2W_{17}O_{61}Zr(\mu\text{-}OH)(H_2O)\}_2]\cdot16H_2O$ revealed two signals at δ −9.72 and −13.74 ppm [72], corresponding to two nonequivalent P atoms in the Wells-Dawson structure. Surprisingly, a quite similar ^{31}P NMR spectrum (δ −10.09 and −13.83 ppm) was reported for the Dawson 1:1 type monomer $(Me_2NH_2)_2H_4[\{\alpha_2\text{-}(H_2O)_2ZrP_2W_{17}O_{61}\}]\cdot8.67H_2O$ in 2 M HCl [83]. The 1:2 complex $K_{15}H[Zr(\alpha_2\text{-}P_2W_{17}O_{61})_2]\cdot25H_2O$ exhibited two resonances at δ −9.20 and −13.81 ppm [81], while for $K_{16}[Zr(\alpha_2\text{-}P_2W_{17}O_{61})_2]\cdot44H_2O$, signals at δ −9.4 and −14.1 ppm were reported [82]. So far, it remained unclear whether the difference in the ^{31}P NMR spectra is due to the distinct counter cations and/or solvent or it is related to the difference in the **Zr-D** polyanion nuclearity (dimer or monomer).

^{31}P NMR spectra of TBA-salts of **Zr-D** collected in dry acetonitrile (Figure 4a) showed a trend consistent with the suggestion about transformation of dimer $[\{\alpha_2\text{-}P_2W_{17}O_{61}Zr(\mu\text{-}OH)\}_2]^{14-}$·(dominated species at pH 3.5–4.5) to monomeric species $[\alpha_2\text{-}P_2W_{17}O_{61}Zr(OH)_n]^{(6+n)-}$ appearing at lower pH. The ^{31}P NMR spectrum of **Zr-D-2.0** reveal two main signals at δ −11.26 and −11.89 ppm. The spectra of samples prepared at pH 2.5 and 3.0 are most complex and show gradual transformation from **Zr-D-2.0** to **Zr-D-3.5**. The spectra of **Zr-D-3.5–4.5** are similar and comprise two sets of resonances, which resemble the spectra of **Zr-D** and **Hf-D** in DMSO reported by Parac-Vogt and co-workers [78]. The splitting of the signals from the two P atoms in the Dawson structure, was rationalized in terms of equilibrium between monomeric 1:1 and dimeric 2:2 species [78]. In principal, it might reflect the presence of two isomeric complexes. However, a geometrical isomer of $[\{\alpha_2\text{-}P_2W_{17}O_{61}Zr(H_2O)_2\}_2]^{12-}$, which consists of two Zr-substituted Dawson units, $[\alpha_2\text{-}P_2W_{17}O_{61}Zr(H_2O)_2]^{6-}$, linked through a Zr–O–W bond, is known to exist at high acidic conditions (pH < 1) [55,83] and, therefore, we can hardly expect it at pH > 3. Moreover, after storing the solution for a

Just Accepted

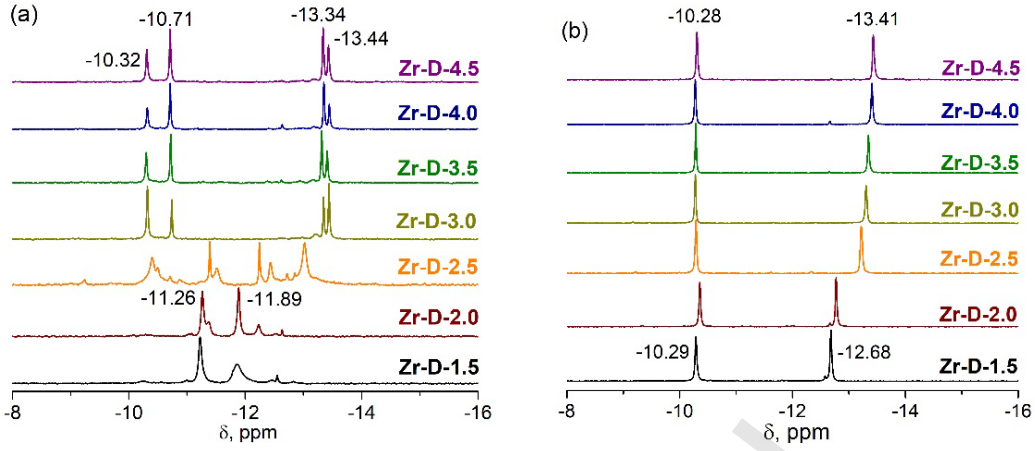


Figure 4 ^{31}P NMR spectra of **Zr-D** (0.01 M solutions, 25 °C): (a) in dry CH_3CN and (b) in CH_3CN + 5 vol% H_2O.

few hours at room temperature, the ratio of the split ^{31}P NMR signals changed in favor of the 'outer' signals and, after 24 hours, only two, 'outer' resonances at –10.30 and –13.41 ppm remained (Figure 2b). It seems that this alteration correlates with the disappearance of the 660 cm^{-1} band in the IR spectra of aged solutions of the samples prepared at pH > 3 (Figure 2a). This might suggest that we deal with a slow process of the 2:2 dimer monomerization producing $[\alpha_2\text{-}P_2W_{17}O_{61}Zr(OH)]^{7-}$ or $[\alpha_2\text{-}P_2W_{17}O_{61}Zr(OH)(H_2O)]^{7-}$. The formation of the latter species may be assisted by adsorption of water from atmosphere upon storage of the acetonitrile solutions. In fact, DFT calculations predict that monomerization of the anhydrous dimer is thermodynamically favorable, with a $\Delta G°$ of –18.3 kcal mol^{-1}, which may account for the spontaneous monomerization observed over time. This hypothesis was further supported by ^{31}P NMR spectra of **Zr-D** run after addition of 5 vol% of water to CH_3CN (Figure 4b). In these spectra, only two resonances associated with the Wells-Dawson structure are observed for all the samples of **Zr-D**, likely, due to fast exchange on the ^{31}P NMR time scale, and the chemical shifts of the ^{31}P NMR signals of**Zr-D-3.5–4.5** in CH_3CN + 5 vol% H_2O coincide with those of **Zr-D-3.5** and **Zr-D-4.5** in the aged CH_3CN solutions (compare spectra in Figures 2b and 4b).

To further investigate these observations, ^{31}P NMR chemical shifts were calculated for the DFT-optimized structures discussed above, and the results are summarized in Figure S6. Among the structures considered, only the aqua-free Zr–hydroxo monomer bearing a proton at a bridging Zr–O–W site reproduces the splitting pattern observed experimentally for freshly prepared **Zr-D-2.0** solutions in dry acetonitrile. This species may arise from partial dehydration of the Zr–triaqua complex upon dissolution in acetonitrile. In agreement with the experimental trends, the calculated separation between the two ^{31}P resonances increases upon hydration to form the Zr–triaqua species (compare the red spectra in Figures 4a and 4b) and becomes even larger for the deprotonated $Zr(OH)(H_2O)$ species. The latter, owing to its higher overall negative charge, is reasonably expected to arise from the synthesis at higher pH, consistent with the observed evolution of the experimental spectra.

What is important, the intensity of the ^{31}P NMR signal of the Zr-free $\{P_2W_{18}\}$ (expected at ca. –12.5 ppm in CH_3CN) was negligible, indicating no conversion of the 2:2 complex to the 1:2 one $[Zr(\alpha_2\text{-}P_2W_{17}O_{61})_2]^{16-}$. Elemental analysis and ESI-MS data for **Zr-D** (see below) also allow the formation of the 1:2 complex to be excluded.

HR-ESI-MS technique was employed to characterize the solution state of **Zr-D**. HR-ESI-MS spectra of dilute (0.001 M) CH_3CN solutions of **Zr-D-2.0** and **Zr-D-4.0** were different despite both represented peaks corresponding to monomeric species (Figure 5; corresponding isotopic patterns are provided in Figures S7 and S8). While the ESI-MS spectrum of **Zr-D-4.0** revealed $TBA_xK_y[P_2W_{17}O_{61}Zr(OH)(H_2O)_n]^{(7-x-y)-}$ (x = 0–5, y = 0–2, n = 0–2) monomers, the spectrum of **Zr-D-2.0** consisted mainly of $TBA_xH_yK_z[P_2W_{17}O_{61}Zr(H_2O)_n]^{(6-x-y-z)-}$ species (x = 0–4, y and z = 0–1, n = 1–2) (alternatively, the formula can be written as $TBA_xH_{y+1}K_z[P_2W_{17}O_{61}Zr(OH)]^{(7-x-y-z)-}$). For both samples, only traces of dimeric species were found. Under similar conditions, **Zr-L** revealed significantly larger fraction of signals associated with dimeric species containing Zr-O(H)-Zr bridges, while **Zr-K** exhibited mainly monomeric species [15,17,89].

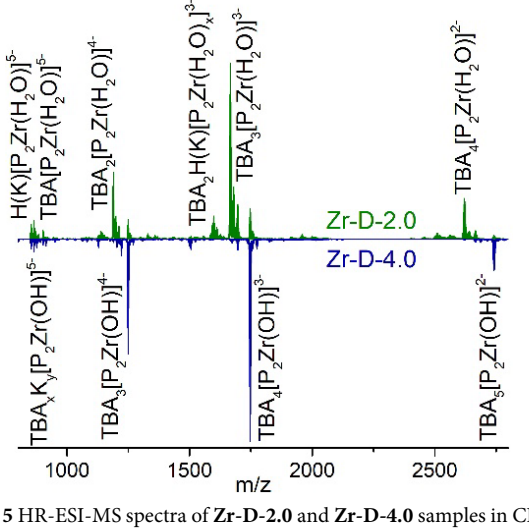


Figure 5 HR-ESI-MS spectra of **Zr-D-2.0** and **Zr-D-4.0** samples in CH_3CN (0.001 M). $P_2Zr = ZrP_2W_{17}O_{61}$.

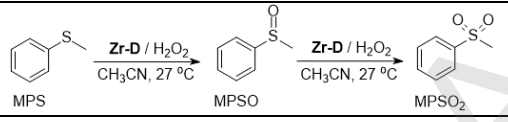
Just Accepted

This is also consistent with the exergonic monomerization energies calculated by DFT for both **Zr-D** ($\Delta G° = -18.3$ kcal mol^{-1}, *vide supra*) and **Zr-K** ($\Delta G° = -3.8$ kcal mol^{-1}). This behavior contrasts sharply with that of **Zr-L**, for which monomerization has been calculated to be slightly endergonic (by 2–4 kcal mol^{-1}) [15,16,86], suggesting a much more pronounced monomer–dimer equilibrium in the latter system, in line with the experimental observations. However, we should remember that ESI-MS signal intensities may depend on both solution speciation and ionization-fragmentation behavior in the source.

3.2. Catalytic performance of Zr-D in thioether oxidation with H_2O_2

The catalytic performance of **Zr-D** synthesized at various pH values was first evaluated in the oxidation of MPS using equimolar amount of aqueous H_2O_2 (Table 1). The efficiency of H_2O_2 utilization was high (85-87%) and independent on the pH of the sample synthesis. In the presence of all **Zr-D**, MPS was converted to the corresponding sulfoxide and sulfone very quickly (within 1–2 minutes). The **Zr-D** samples synthesized at pH 3.0 and 4.0 showed nearly identical performance in terms of activity (TOF 43 min^{-1}) and selectivity to sulfoxide (72%). The samples prepared at pH 1.5 and 2.0 revealed both higher activity (TOF 210–220 min^{-1}) and sulfoxidation selectivity (77–82%). The selectivity of **Zr-D-2.0** was close to that reported previously for the diperoxo complex **Zr(O_2)-D** [19], but the H_2O_2 utilization efficiency of the latter was inferior (77 vs 85%).

Table 1 MPS oxidation with H_2O_2 in the presence of **Zr-D**[a]

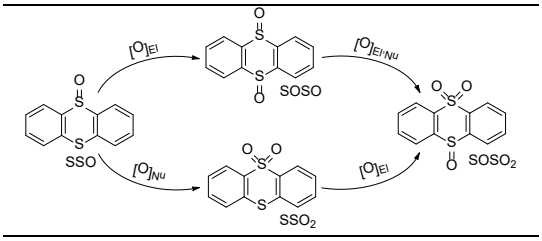


POM	Time, min	MPS conv., %	TOF, min^{-1}	Selectivity, %		H_2O_2 eff.,[c] %
				MPSO	$MPSO_2$	
Zr-D-1.5	1	70	210	77	23	86
Zr-D-2.0	1	72	220	82	18	85
Zr-D-3.0	2	68	43	72	28	87
Zr-D-4.0	2	67	43	72	28	86
Zr(O_2)-D[d]	1	65	-	82	18	77

[a]Reaction conditions: Zr 0.002 M, MPS 0.1 M, H_2O_2 (30% aq.) 0.1 M, CH_3CN 1 mL, 27 °C. [b]Turnover frequency (TOF) was determined from initial rates of MPS consumption. [c]H_2O_2 efficiency was calculated as total yield of products (MPSO + 2·$MPSO_2$) based on the oxidant consumed. [d]Data taken from ref. [19].

The oxidation of thianthrene-5-oxide (SSO), a well-known mechanistic probe to evaluate electronic properties of the oxidizing species [90,91], was also performed. The reaction conditions were chosen to keep conversion of SSO below 15% since overoxidation of the primary oxidation products, SOSO (electrophilic oxidation) and SSO_2 (nucleophilic oxidation) to $SOSO_2$ can mask the information on the chemoselectivity and affect the value of the nucleophilic parameter X_{Nu} [91]. The results acquired for the SSO oxidation (Table 2) indicate a stronger electrophilic character of the oxidizing species formed from **Zr-D-2.0** (X_{Nu} = 0.12 vs 0.21 for **Zr-D-4.0**). Under the same conditions, a similar parameter X_{Nu} was obtained for **Zr-K** while **Zr-L** revealed X_{Nu} of 0.29 (Table 2), indicating a lower electrophilicity. Walls et al. recently reported X_{Nu} 0.09 for **ZrV_5** [63].

Table 2 Oxidation of SSO with H_2O_2 in the presence of **Zr-D**[a]



POM	SSO conv., %	Yields, %			X_{Nu}[b]
		SOSO	SSO_2	$SOSO_2$	
Zr-D-2.0	15	13	1	1	0.12
Zr-D-4.0	13	10	2	1	0.21
Zr-K	15	13	1	1	0.12
Zr-L	6.5	4.3	1	1.2	0.29

[a]Reaction conditions: Zr 0.0005 M, SSO 0.025 M, H_2O_2 (30% aq.) 0.0038 M, CH_3CN 2 mL, 27 °C, 10 min. [b]X_{Nu} = (SSO_2 + $SOSO_2$)/(SOSO + SSO_2 + 2$SOSO_2$) [91].

Given that both **Zr-D-2.0** and **Zr-D-4.0** are monomers in dilute solutions (see above), the difference in activity and selectivity of **Zr-D-2.0** and **Zr-D-4.0** can be, in principle, rationalized if we remember that the former comprises additional proton, which decreases the polyanion negative charge and makes the corresponding active species more electrophilic. Earlier, we demonstrated that protonation of Ti-POM decreases an oxygen transfer barrier to C=C bonds due to the global charge effect [92]. DFT calculations revealed that location of proton on a Zr–O–W in **Zr-D** is energetically more feasible than its location at the terminal Zr–OH; however, additional hydration reduces free energy of Zr species with terminal water ligands (Scheme 1). The nature of terminal Zr ligand (H_2O vs OH) may affect the structure of peroxo species formed upon interaction with H_2O_2. This matter will be discussed in our subsequent work.

3.3. Effect of negative charge density on the catalytic performance of Zr-POMs

If we compare the catalytic performance of **Zr-D** with those previously reported for Zr-POMs of the Lindqvist [15] and Keggin [18] structures, we can see that, in terms of activity in the MPS oxidation, **Zr-D** occupies an intermediate position between **Zr-L** and **Zr-K** (Figure 6a). For **Zr-K**, the MPS conversion reaches its maximum after 15 sec. while the reaction with **Zr-L** requires ca. 30 min. It is noteworthy that the same trend is observed if H_2O_2 is replaced with *tert*-butyl hydroperoxide (TBHP; Figure 6b).

The MPS oxidation activity appears to correlate inversely with the polyanion charge density (q/M, the overall polyanion negative charge per number of metal atoms), which decreases in the order: **Zr-L** (0.50) > **Zr-D-4.0** (0.39) > **Zr-K** (0.33) (Figure 7). This global feature is also reflected in the local electronic environment of the catalytic Zr center, with increasing positive charge on Zr for the different species: **Zr-L** (+1.83 *e*) < **Zr-D-4.0** (+1.90 *e*) < **Zr-K** (+1.94 *e*), using NPA population analysis. Thus, **Zr-L** has the highest polyanion charge density and displays the least positive Zr

Just Accepted

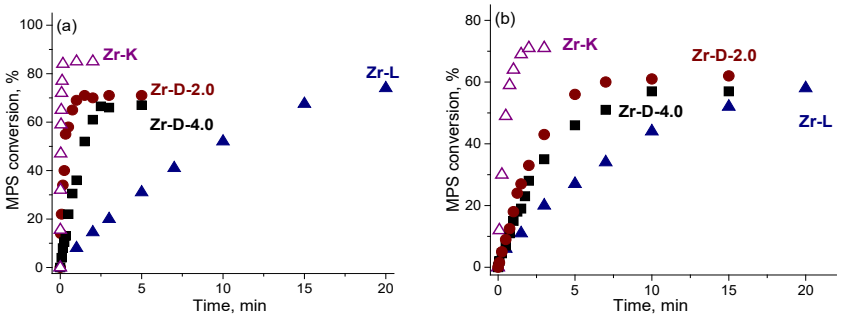


Figure 6 Kinetic profiles for MPS conversion in MPS oxidation with (a) H_2O_2 and (b) TBHP in the presence of Zr-POMs. Reaction conditions: Zr 0.002 M, MPS 0.1 M, H_2O_2 or TBHP 0.1 M, CH_3CN 1 mL, 27 °C. For TBHP, the data were taken from [93].

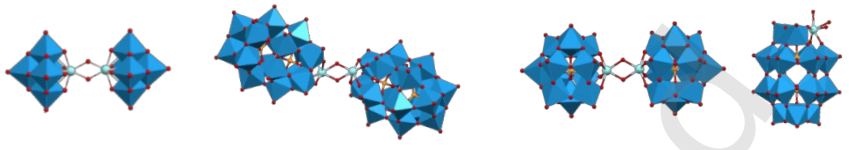


Figure 7 Structures of Zr-POMs and corresponding polyanion charge density values.

center and the lowest catalytic activity, whereas **Zr-K** exhibits the most positive Zr center and the highest activity. **Zr-D** structures display intermediate polyanion charge densities and Zr positive charges, consistent with its intermediate catalytic performance. Although polyoxometalate charge density is a primary factor affecting catalytic activity, we cannot discard other influences such as the specific coordination environment of Zr along the series.

While thioethers are strong nucleophiles, sulfoxides possess a biphilic nature and can react with both electrophilic and nucleophilic oxidants [94]. In the oxidation of corresponding sulfoxide to sulfone, a similar correlation of Zr-POM activity with q/M was found (Figure S9), indicating that in both stages we deal with electrophilic oxygen transfer (the lower negative charge density, the more favorable interaction with nucleophilic substrate).

In sulfoxide oxidation, **Zr-K** and **Zr-D-2.0** catalysts, with the same q/M of 0.33, have similar activity (Figure S9), whereas for MPS oxidation, **Zr-K** is somewhat more active than **Zr-D-2.0** (Figure 6a). These results suggest that other factors, such as the specific POM framework, size and shape, local Zr coordination, hydration state, as well as monomer-dimer equilibrium can also modulate the catalytic performance, with the overall POM charge density being a key factor.

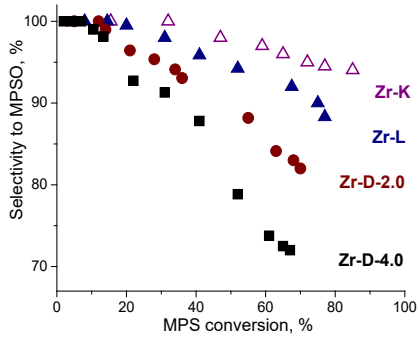


Figure 8 Dependence of MPSO selectivity on substrate conversion in MPS oxidation with H_2O_2 in the presence of Zr-POMs.

At the initial stages of the reaction, sulfoxidation selectivity is *ca.* 100% for all Zr-POMs studied but, if we compare selectivity trends observed for **Zr-D**, **Zr-K** and **Zr-L**, we can see that, during the reaction course, sulfoxide selectivity is higher for **Zr-K** and lower for **Zr-D**, while **Zr-L** occupies an intermediate position (Figure 8). This is different from what we observed for the MPS oxidation with TBHP where sulfoxidation selectivity inversely correlated with the Zr-POM charge density [93]. The lowest selectivity found for **Zr-L** was explained by its higher affinity toward sulfoxide, which favored overoxidation to sulfone. As to the MPS oxidation with H_2O_2, we may tentatively assume that the increased sulfoxide selectivity of **Zr-L** can be caused by the side reaction of the oxidant decomposition. Our previous work revealed that, among the series of Zr-POMs, **Zr- L** shows superior activity in H_2O_2 dismutation and this process proceeds with release of singlet oxygen [16], which can contribute to the oxidation process [20].

Interestingly, in the oxidation of SSO, which was investigated at the deficiency of H_2O_2 relative to the substrate to minimize overoxidation of the primary oxidation products and the oxidant decomposition, the parameter X_{Nu} that reflects the oxidation selectivity correlated directly with Zr-POM charge density (Figure 9).

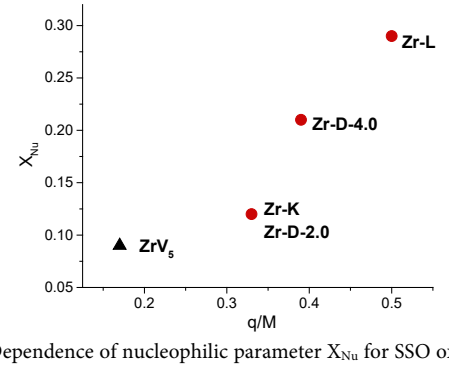


Figure 9 Dependence of nucleophilic parameter X_{Nu} for SSO oxidation on polyanion charge density for Zr-POMs (data for **ZrV_5** taken from ref. [63]).

Just Accepted

Moreover, X_{Nu} reported for **ZrV$_5$** [63] also fell into this correlation (Figure 9).

4 Conclusions

The detailed experimental and computational characterization of the series of **Zr-D** samples and assessment of their catalytic performance in selective oxidation of thioethers clearly demonstrated that acidity of the solution before precipitation of the TBA salt plays a crucial role for both composition/structure and catalytic activity/selectivity of **Zr-D**. Whereas **Zr-D** prepared at pH 1.5–2.0 exist preferably in the form of the monomer $[\alpha_2\text{-}P_2W_{17}O_{61}Zr(H_2O)_3]^{6-}$, **Zr-D** obtained at pH 3.5–4.5 are mostly dimers $[\{P_2W_{17}O_{61}Zr(\mu\text{-}OH)\}_2]^{14-}$ in the solid state and monomerize to $[\alpha_2\text{-}P_2W_{17}O_{61}Zr(OH)]^{7-}$ in dilute acetonitrile solutions. Monomer **Zr-D-2.0** contains terminal water and, as a result, has additional proton relative to **Zr-D-4.0**, which increases its electrophilicity and ensures higher activity and sulfoxidation selectivity in the thioether oxidation.

Comparison of the catalytic performance of Zr-POMs with different structural type (Lindqvist, Keggin and Wells-Dawson) present in the same protonation state revealed that activity of **Zr-D** is intermediate between **Zr-K** and **Zr-L**. The observed structural effect can be rationalized in terms of the polyanion charge density, which decreases in the order **Zr-L** > **Zr-D** > **Zr-K**, and are inversely correlated to the catalytic activity with **Zr-K** being the most active species, more directly, with the calculated positive charge at the Zr center, supporting a key role of Zr electrophilicity in determining catalytic activity. Nonetheless, other factors related to the specific POM framework can also influence the activity to a minor extend, opening new venues for future mechanistic studies.

Electronic Supplementary Material: Supplementary material (additional experimental details, synthesis procedures, FT-IR, NMR, and HR-ESI-MS spectra, TGA curves, potentiometric titration curves, and kinetic curves) is available in the online version of this article at https://doi.org/10.26599/POM.2026.9140172.

Data availability

All data needed to support the conclusions in the paper are presented in the manuscript and/or the Electronic Supplementary Material. Additional data related to this paper may be requested from the corresponding author upon request.

Acknowledgements

We dedicate this work to the memory of POM pioneer Professor Michael Pope who passed away recently. The authors thank Dr I. E. Soshnikov for ^{1}H NMR measurements. The studies were carried out using facilities of the shared research center "National center of investigation of catalysts" at the Boreskov Institute of Catalysis and the Center of Collective Use "Mass spectrometric investigations" SB RAS. This work was supported by the Russian Science Foundation (No. 23-13-00156-П, https://rscf.ru/en/project/23-13-00156-П/). J. P.-J., A. S.-D. and J. J. C. thank grant PID2024-162773NB-I00 funded by MCIN/AEI/10.13039/501100011033 and by "ERDF A way of making Europe" and the European Union NextGenerationEU/PRTR.

Declaration of competing interest

All the contributing authors report no conflict of interests in this work.

Author contribution statement

S.M.M.: experimental design, investigation, data curation, visualization, and writing–original draft. N.V.M.: conceptualization, investigation, data curation, and writing–original draft. O.V.Z.: investigation, formal analysis, and writing–review & editing. V.Y.E.: data curation and writing–review & editing. A.A.A.: investigation and formal analysis. J.P.-J.: formal analysis, visualization, and writing–review & editing. A.S.-D.: formal analysis, visualization, and writing–review & editing V.V.Y.: investigation and formal analysis. J.J.C.: conceptualization and writing–review & editing. O.A.K.: supervision, conceptualization, funding acquisition, and writing–review & editing. All authors contributed to reviewing and editing this document. All authors have given approval to the final version of the manuscript.

Use of AI statement

None.

References

[1] Sheldon, R. A.; Van Doorn, J. A. Metal-catalyzed epoxidation of olefins with organic hydroperoxides: I. A Comparison of Various Metal Catalysts. *J. Catal.* **1973**, *32*, 427–437.

[2] Bregante, D. T.; Flaherty, D. W. Periodic trends in olefin epoxidation over group IV and V framework-substituted zeolite catalysts: A Kinetic and Spectroscopic Study. *J. Am. Chem. Soc.* **2017**, *139*, 6888–6898

[3] Besson, M.; Bonnet, M. C.; Gallezot, P.; Tkatchenko, I.; Tuel, A. Catalysis for fine chemicals: towards specificity with polyphasic media. *Catal. Today* **1999**, *51,* 547–560.

[4] Maksimchuk, N. V.; Melgunov, M. S.; Mrowiec-Białoń, J.; Jarzębski, A. B.; Kholdeeva, O. A. H_2O_2-Based allylic oxidation of α-pinene over different single site catalysts. *J. Catal.* **2005**, *235,* 175–183.

[5] Ivanchikova, I. D.; Zalomaeva, O. V.; Maksimchuk, N. V.; Stonkus, O. A.; Glazneva, T. S.; Chesalov, Yu. A.; Shmakov, A. N.; Guidotti, M.; Kholdeeva, O. A. Alkene epoxidation and thioether oxidation with hydrogen peroxide catalyzed by mesoporous zirconium-silicates. *Catalysts* **2022** *12*, 742.

[6] Cavka, J. H.; Jakobsen, S.; Olsbye, U.; Guillou, N.; Lamberti, C.; Bordiga, S.; Lillerud, K.P. A New ZIrconium inorganic building brick forming metal organic frameworks with exceptional stability. *J. Am. Chem. Soc.* **2008**, *130*, 13850–13851.

[7] Dhakshinamoorthy, A.; Navalon, S.; Asiri, A.M.; Garcia, H. Metal organic frameworks as solid catalysts for liquid-phase continuous flow reactions. *Chem. Commun.* **2020**, *56*, 26–45.

[8] Dhakshinamoorthy, A.; Santiago-Portillo, A.; Asiri, A.M.; Garcia, H. Engineering UiO-66 Metal organic framework for heterogeneous catalysis. *ChemCatChem* **2019**, *11*, 899–923.

[9] Limvorapitux, R.; Chen, H.; Mendonca, M. L.; Liu, M.; Snurr, R. Q.; Nguyen, S.T. Elucidating the mechanism of the UiO-66-catalyzed sulfide oxidation: activity and selectivity enhancements through changes in the node coordination environment and solvent. *Catal. Sci. Technol.* **2019**, *9*, 327–335.

[10] Maksimchuk, N. V.; Lee, J.S.; Solovyeva, M. V.; Cho, K. H.; Shmakov, A. N.; Chesalov, Y. A.; Chang, J.-S.; Kholdeeva, O. A. Protons make possible heterolytic activation of hydrogen peroxide over Zr-based metal-organic frameworks. *ACS Catal.* **2019**, *9*, 9699–9704.

[11] Zalomaeva, O. V.; Evtushok, V. Yu.; Ivanchikova, I. D.; Glazneva, T. S.; Chesalov, Yu. A.; Larionov, K. P.; Kholdeeva, O. A. Nucleophilic vs electrophilic activation of hydrogen peroxide over Zr-based metal-organic frameworks. *Inorg. Chem.* **2020**, *59*, 10634–10649.

[12] Maksimchuk, N. V.; Ivanchikova, I. D.; Cho, K. H.; Zalomaeva, O. V.; Evtushok, V. Y.; Larionov, K. P.; Glazneva, T. S.; Chang, J.-S.; Kholdeeva, O. A. Catalytic performance of Zr-based metal-organic frameworks Zr-abtc

Just Accepted

and MIP-200 in selective oxidations with H_2O_2. *Chem. Eur. J.* **2021**, *27*, 6985–6992.
[13] Kholdeeva, O. A.; Maksimchuk, N. V. Metal-organic frameworks in oxidation catalysis with hydrogen peroxide. *Catalysts* **2021**, *11*, 283.
[14] Evtushok, V. Yu.; Larionov, K. P.; Lopatkin, V. A.; Stonkus, O. A.; Kholdeeva, O. A. What factors determine activity of UiO-66 in H_2O_2-based oxidation of thioethers? The role of basic sites. *J. Catal.* **2023**, *427*, 115099.
[15] Maksimchuk, N. V.; Evtushok, V. Yu.; Zalomaeva, O. V.; Maksimov, G. M.; Ivanchikova, I. D.; Chesalov, Yu. A.; Eltsov, I. V.; Abramov, P. A.; Glazneva, T. S.; Yanshole, V. V.; Kholdeeva, O. A.; Errington, R. J.; Solé-Daura, A.; Poblet, J. M.; Carbó, J. J. Activation of H_2O_2 over Zr(IV). Insights from model studies on Zr-monosubstituted Lindqvist tungstates. *ACS Catal.* **2021**, *11*, 10589–10603.
[16] Maksimchuk, N. V.; Puiggalí-Jou, J.; Zalomaeva, O. V.; Larionov, K. P.; Evtushok, V. Yu.; Soshnikov, I. E.; Solé-Daura, A.; Kholdeeva, O. A.; Poblet, J. M.; Carbó, J. J. Resolving the mechanism for H_2O_2 decomposition over Zr(IV)-substituted Lindqvist tungstate: evidence of singlet oxygen intermediacy. *ACS Catal.* **2023**, *13*, 10324–10339.
[17] Maksimchuk, N. V.; Marikovskaya, S. M.; Larionov, K. P.; Antonov, A. A.; Shashkov, M. V.; Yanshole, V. V.; Evtushok, V. Yu.; Kholdeeva, O. A. Tuning reactivity of Zr-substituted Keggin phosphotungstate in alkene epoxidation through balancing H_2O_2 activation pathways: unusual effect of base. *Inorg. Chem.* **2023**, *62,* 18955–18969.
[18] Zalomaeva, O. V.; Maksimchuk, N. V.; Marikovskaya, S. M.; Antonov, A. A.; Kholdeeva, O. A. Highly selective thioether oxidation with H_2O_2 catalyzed by Zr-substituted Keggin phosphotungstate: mechanistic insights. *ChemCatChem* **2024**, *16*, e202301374.
[19] Sundar, A.; Maksimchuk, N. V.; Ivanchikova, I. D.; Zalomaeva, O. V.; Bajuk-Bogdanović, D.; Kholdeeva, O. A.; Ćirić-Marjanović, G.; Bassil, B. S.; Kortz, U. Peroxo-Zr/Hf-containing Wells-Dawson polyoxometalates for H_2O_2-based homogeneous, heterogeneous, and biphasic oxidation Catalysis. *Chem. Europe* **2024**, *2*, e202300066.
[20] Maksimchuk, N. V.; Marikovskaya, S. M.; Larionov, K. P.; Evtushok, V. Yu.; Yanshole, V. V.; Antonov, A. A.;Kholdeeva, O. A. Effect of the polyanion structure on the mechanism of alcohol oxidation with H_2O_2 catalyzed by Zr-substituted polyoxotungstates, *Inorg.Chem.* **2024**, *63*, 18043–18057.
[21] Pope, M. T. *Heteropoly and Isopoly Oxometalates*; Springer Verlag: Berlin, 1983.
[22] Pope, M. T. Polyoxo Anions: Synthesis and Structure. In *Comprehensive Coordination Chemistry II*; Wedd, A. G., Ed.; Elsevier Science, New York, 2004; Vol. 4, pp 635–678.
[23] Miras, H. N.; Yan, J.; Long, D.-L.; Cronin, L. Engineering polyoxometalates with emergent properties, *Chem. Soc. Rev.* **2012**, *41*, 7403–7430.
[24] Liu, R.; Streb, C. Polyoxometalate-single atom catalysts (POM-SACs) in energy research and catalysis, *Adv. Energy Mater.* **2021**, *11*, 2101120.
[25] Zhang, S.; Liu, R.; Streb, C.; Zhang, G. Design and synthesis of novel polyoxometalate-based binary and ternary nanohybrids for energy conversion and storage, *Polyoxometalates* **2023**, *2*, 9140037.
[26] Granadeiro, C. M.; Julião, D.; Ribeiro, S. O.; Cunha-Silva, L.; Balula, S.S. Recent advances in lanthanide-coordinated polyoxometalates: from structural overview to functional materials, *Coord. Chem. Rev.* **2023**, *476*, 214914.
[27] Yang, Z.; Li, J.; Niu, J.; Wang, J. Polyoxotantalate chemistry: from synthetic strategies to structural diversity and applications, *Dalton Trans.* **2023**, *52*, 4632–4642.
[28] Wang, M.; Pang, J.; Wang, J.; Niu, J. Recent advances in mono-lacunary Keggin- type polyoxometalate-based crystalline materials: from synthetic strategies, diverse structures to functional applications, *Coord. Chem. Rev.* **2024**, *508*, 215730.
[29] Gao, A.; Iwano, T.; Uchida, S. Emerging functionalized Lindqvist-type polyoxometalate-based compounds: design, synthesis, and applications, *ChemCatChem* **2025**, *17*, e202500066.
[30] Bijelic, A.; Aureliano, M.; Rompel, A. Polyoxometalates as potential next-generation metallodrugs in the combat against cancer, *Angew. Chem. Int. Ed*. **2019**, *58*, 2980–2999.
[31] Wózniak Budych, M. J.; Staszak, K.; Bajek, A.; Pniewski, F.; Jastrząb, R.; Staszak, M.; Tylkowski, B.; Wieszczycka, K. The future of polyoxymetalates for biological and chemical applications, *Coord. Chem. Rev.* **2023**, *493*, 215306.
[32] Lentink, S.; Salazar Marcano, D. E.; Moussawi, M. A.; Parac-Vogt, T. N. Exploiting interactions between polyoxometalates and proteins for applications in (bio) chemistry and medicine, *Angew. Chem. Int. Ed.* **2023**, *62*, e202303817.
[33] Van Rompuy, L. S.; Parac-Vogt, T. N. Interactions between polyoxometalates and biological systems: from drug design to artificial enzymes, current opinion, *Biotechnol 58* (**2019**) 92–99.
[34] Wang, S.-S.; Yang, G.-Y. Recent advances in polyoxometalate-catalyzed reactions, *Chem. Rev*. **2015**, *115*, 4893–4962.
[35] Lechner, M.; Güttel, R.; Streb, C. Challenges in polyoxometalate-mediated aerobic oxidation catalysis: catalyst development meets reactor design, *Dalton Trans.* **2016**, *45*, 16716–16726.
[36] Weinstock, I. A.; Schreiber, R. E.; Neumann, R. Dioxygen in polyoxometalate mediated reactions, *Chem. Rev*. **2018**, *118*, 2680–2717
[37] Kamata, K.; Sugahara, K.Base catalysis by mono- and polyoxometalates, *Catalysts* **2017**, *7,* 345.
[38] Lauinger, S. M.; Yin, Q.; Geletii, Y. V. Hill, C. L. Polyoxometalate multielectron catalysts in solar fuel production, *Adv. Inorg. Chem.* **2017**, *69,* 117–154
[39] Suzuki, K.; Mizuno, N.; Yamaguchi, K. Polyoxometalate photocatalysis for liquid- phase selective organic functional group transformations, *ACS Catal.* **2018**, *8*, 10809–10825.
[40] Han, Q.; Ding, Y. Recent advances in the field of light-driven water oxidation catalyzed by transition-metal substituted polyoxometalates, *Dalton Trans.* **2018**, *47*, 8180–8188.
[41] de Azambuja, F.; Moons, J.; Parac-Vogt, T. N. The dawn of metal-oxo clusters as artificial proteases: from discovery to the present and beyond, *Acc. Chem. Res.* **2021**, *54,* 1673–1684
[42] Aramesh, N.; Bagheri, A. R.; Zhang, Z.; Yadollahi, B.; Lee, H. K. Polyoxometalate- based materials against environmental pollutants: a review, *Coord. Chem. Rev.* **2024**, *507,* 215767.
[43] Hu, Q.; Zhou, H.; Ding, Y.; Wagberg, T.; Han, X. Advances in bridging homogeneous and heterogeneous water oxidation catalysis by insolubilized polyoxometalate clusters, *ACS Catal.* **2024**, *14,* 5898–5910.
[44] Maksimchuk, N. V.; Kholdeeva, O. A. Heterolytic Activation of hydrogen peroxide and selective oxidations with d^0-heterometallic polyoxometalates: recent advances and mechanistic insights. *Coord. Chem. Rev.* **2026**, *547,* 217108.
[45] Fournier, M.; Louis, C.; Che, M.; Chaquin, P.; Masure, D. Polyoxometallates as models for oxide catalysts Part I. An UV-visible reflectance study of polyoxomolybdates: Influence of polyhedra arrangement on the electronic transitions and comparison with supported molybdenum catalysts. *J. Catal.* **1989**, *119*, 400–414.
[46] Thomas, J.M. *Design and Applications of Single-Site Heterogeneous Catalysts: Contributions to Green Chemistry, Clean Technology and Sustainability*; Imperial College Press: London, U.K.; 2012.
[47] Villanneau, R.; Carabineiro, H.; Carrier, X.; Thouvenot, R.; Herson, P.; Lemos, F.; Ramôa Ribeiro, F.; Che, M. Synthesis and characterization of Zr(IV) polyoxotungstates as molecular analogues of zirconia-supported tungsten catalysts. *J. Phys. Chem. B* **2004**, *108*, 12465–12471.
[48] Carabineiro, H.; Villanneau, R.; Carrier, X.; Herson, P.; Lemos, F.; Ramôa Ribeiro, F.; Proust, A.; Che, M. Zirconium-substituted isopolytungstates: structural models for zirconia-supported tungsten catalysts. *Inorg. Chem*. **2006**, *45*, 1915–1923.
[49] Kholdeeva, O. A. Titanium-monosubstituted polyoxometalates: relation between homogeneous and heterogeneous Ti-single-site based catalysis. *Top. Catal.* **2006**, *40*, 229–243.
[50] Kholdeeva, O. A. Hydrogen peroxide activation over Ti^{IV}: what have we learned from studies on Ti-containing polyoxometalates? *Eur. J. Inorg. Chem*. **2013**, 1595–1605.
[51] Guillemot, G.; Matricardi, E.; Chamoreau, L.-M.; Thouvenot, R.; Proust, A. Oxidovanadium(V) anchored to silanol-functionalized polyoxotungstates: molecular models for single-site silica-supported vanadium catalysts. *ACS Catal.* **2015**, *5*, 7415–7423.
[52] Zhang, T.; Mazaud, L.; Chamoreau, L.-M.; Paris, C.; Proust, A.; Guillemot, G. Unveiling the active surface sites in heterogeneous titanium-based silicalite epoxidation catalysts: input of silanol functionalized polyoxotungstates as soluble analogues. *ACS Catal.* **2018**, *8*, 2330–2342.
[53] Solé-Daura, A.; Zhang, T.; Fouilloux, H.; Robert, C.; Thomas, C. M.; Chamoreau, L.-M.; Carbó, J. J.; Proust, A.; Guillemot, G.; Poblet, J. M.

Just Accepted

Catalyst design for alkene epoxidation by molecular analogues of heterogeneous titanium-silicalite Catalysts. *ACS Catal.* **2020**, *10*, 4737−4750.

[54] Solé-Daura, A.; Carbó, J. J. Computational modeling of the epoxidation of alkenes with hydrogen peroxide catalyzed by transition metal-substituted polyoxometalates, *Adv. Catal.* **2024**, *75*, 95–129.

[55] See for review Nomiya, K.; Sakai, Y.; Matsunaga, S. Chemistry of Group IV Metal Ion-Containing Polyoxometalates. *Eur. J. Inorg. Chem.* **2011**, 179–196.

[56] Ni, Z.; Lv, H.; Yang, G. Recent advances of Ti/Zr-substituted polyoxometalates: from structural diversity to functional applications. *Molecules* **2022**, *27*, 8799.

[57] Kholdeeva, O. A.; Maksimov, G. M.; Maksimovskaya, R. I.; Vanina, M. P.; Trubitsina, T. A.; Naumov, D. Y.; Kolesov, B. A.; Antonova, N. S.; Carbó, J. J.; Poblet, J. J. Zr^{IV}-monosubstituted Keggin-type dimeric polyoxometalates: synthesis, characterization, catalysis of H_2O_2-Based oxidations, and theoretical study. *Inorg. Chem.* **2006**, *45*, 7224–7234.

[58] Al-Kadamany, G.; Sankar Mal, S.; Milev, B.; Donoeva, B. G.; Maksimovskaya, R. I.; Kholdeeva, O. A.; Kortz, U. Hexazirconium- and hexahafnium-containing tungstoarsenates(III) and their oxidation catalysis properties. *Chem. Eur. J.* **2010**, *16*, 11797–11800.

[59] Aoto, H.; Matsui, K.; Sakai, Y.; Kuchizi, T.; Sekiya, H.; Osada, H.; Yoshida, T.; Matsunaga, S.; Nomiya, K. Zirconium(IV)- and hafnium(IV)-containing polyoxometalates as oxidation precatalysts: homogeneous catalytic epoxidation of cyclooctene by hydrogen peroxide. *J. Mol. Catal. A: Chem*. **2014**, *394,* 224–231.

[60] Bassil, B. S.; Sankar Mal, S.; Dickman, M.H.; Kortz, U.; Oelrich, H.; Walder, L. 6-Peroxo-6-zirconium crown and its hafnium analogue embedded in a triangular polyanion: $[M_6(O_2)_6(OH)_6(\gamma\text{-}SiW_{10}O_{36})_3]^{18-}$ (M = Zr, Hf). *J. Am. Chem. Soc.* **2008**, *130*, 6696–6697.

[61] Carraro, M.; Nsouli, N.; Oelrich, H.; Sartorel, A.; Sorar, A.; Sankar Mal, S.; Scorrano, G.; Walder, L.; Kortz, U.; Bonchio, M.; Reactive Zr^{IV} and Hf^{IV} butterfly peroxides on polyoxometalate surfaces: bridging the gap between homogeneous and heterogeneous catalysis. *Chem. Eur. J.* **2011**, *17*, 8371–8378.

[62] Sankar Mal, S.; Nsouli, N.H.; Carraro, M.; Sartorel, A.; Scorrano, G.; Oelrich, H.; Walder, L.; Bonchio, M.; Kortz, U. Peroxo-Zr/Hf-containing undecatungstosilicates and –germinates. *Inorg. Chem.* **2010**, *49,* 7–9.

[63] Walls, M. R. A.; Clark, K.; Cooney, S. E.; Brennessel, W. W.; Matson E. M. Isolation of a rare terminal Zr(IV) peroxide and insight into polyoxovanadate support impacton thioether oxidation. *Chem. Eur. J.* **2025**, 31, e202404550.

[64] Huang, L. ; Wang, S.-S.; Zhao, J.-W.; Cheng, L.; Yang, G.-Y. Synergistic combination of multi-Zr^{IV} cations and lacunary Keggin germanotungstates leading to a gigantic Zr_{24}-cluster-substituted polyoxometalate. *J. Am. Chem. Soc.* **2014**, *136*, 7637–7642.

[65] Wang, Y.-L.; Zhang, Z.; Li, H.-L.; Li, X.-Y.; Yang, G.-Y. An oxalate-functionalized tetra-Zr^{IV}-substituted sandwich-type silicotungstate: Hydrothermal synthesis, structural characterization, and catalytic oxidation of thioethers. *Eur. J. Inorg. Chem*. **2019**, 417–422.

[66] Wang, Y.-L.; Yang, G.-Y. Two α_2-monozirconium-substituted dimeric silicotungstates: Hydrothermal synthesis, structural characterization and catalytic oxidation of thioethers. *J. Cluster Sci.* **2019**, *30,* 1115–1121

[67] Zhang, Z.; Wang, Y.-L.; Liu, Y.; Huang, S.-Li.; Yang, G.-Y. Three ring-shaped Zr(IV)-substituted silicotungstates: syntheses, structures and their properties. *Nanoscale,* **2020,** *12,* 18333–18341.

[68] Li, H.-L.; Lian, C.; Yin, D.-P.; Yang, G.-Y. Three Zr(IV)-substituted polyoxotungstate aggregates: Structural transformation from tungstoantimonate to tungstophosphate induced by pH. *Inorg. Chem.* **2020**, *59*, 12842–12849.

[69] Zhang, P.-Y.; Wang, Y.; Yao, L.-Y.; Yang, G.-Y. Hepta-Zr-incorporated polyoxometalate assembly, *Inorg. Chem.* **2022**, *61*, 10410–10416.

[70] Sheng, Y.-H.; Sun, J.-J.; Zhang, P.-Y.; Yang, G.-Y. A Zr-substituted polyoxotungstate built by $[\beta\text{-}GeW_{10}O_{38}]^{12-}$ and $[A\text{-}\alpha\text{-}PW_9O_{34}]^{9-}$ fragments: Synthesis, structure and properties. *J. Cluster Sci.* **2022**, *33*, 1677–1684.

[71] Yang, D.;Li, Z.; Lian, Y.; Fu, Z.; Li, T.; Ma, P.; Yang, G. A novel square-shaped Zr-substituted polyoxotungstate for the efficient catalytic oxidation of sulfide to sulfone. *Chin. Chem. Lett.* **2025**, *36*, 109717.

[72] Saku, Y.; Sakai, Y.; Nomiya, K. Relation among the 2:2-, 1:1- and 1:2-type complexes of hafnium(IV)/zirconium(IV) with mono-lacunary α_2-dawson polyoxometalate ligands: synthesis and structure of the 2:2-type complexes $[\{\alpha_2\text{-}P_2W_{17}O_{61}M(\mu\text{-}OH)(H_2O)\}_2]^{14-}$ (M = Hf, Zr). *Inorg. Chim. Acta* **2010**, *363*, 967–974.

[73] Nowicka, D.; Vadra, N.; Wieczorek-Szweda, E.; Patroniak, V.; Gorczyński, A. Overview of Wells-Dawson polyoxometalates: from structure and functionalization to application. *Coord. Chem. Rev.* **2024**, *519,* 216091.

[74] Dupré, N.; Remy, P.; Micoine, K.; Boglio, C.; Thorimbert, S.; Lacôte, Hasenknopf, B.; Malacria, M. Chemoselective catalysis with organosoluble lewis acidic polyoxotungstates. *Chem. Eur. J.* **2010**, *16*, 7256–7264.

[75] Vanhaecht, S.; Absillis, G.; Parac-Vogt, T. N. Amino acid side chain induced selectivity in the hydrolysis of peptides catalyzed by a Zr(IV)-substituted Wells–Dawson type polyoxometalate. *Dalton Trans.* **2013**, *42*, 15437–15446.

[76] Sap, A.; Absillis, G.; Parac-Vogt, T. N. Selective hydrolysis of oxidized insulin chain B by a Zr(IV)-substituted Wells–Dawson polyoxometalate. *Dalton Trans.* **2015**, *44*, 1539–1548.

[77] Stroobants, K.; Goovaerts, V.; Absillis, G.; Bruylants, G.; Moelants, E.; Proost, P.; Parac-Vogt, T. N. Molecular origin of the hydrolytic activity and fixed regioselectivity of a Zr^{IV}-substituted polyoxotungstate as artificial protease. *Chem. Eur. J.* **2014**, *20*, 9567–9577.

[78] de Azambuja, F.; Parac-Vogt, T. N. Water-tolerant and atom economical amide bond formation by metal-substituted polyoxometalate catalysts. *ACS Catal.* **2019**, *9*, 10245–10252.

[79] Absillis, G.; Parac-Vogt, T. N. Peptide bond hydrolysis catalyzed by the Wells–Dawson $Zr(\alpha_2\text{-}P_2W_{17}O_{61})_2$ polyoxometalate. *Inorg. Chem.* **2012**, *51*, 9902–9910.

[80] Bonchio, M.; Conte, V.; Deconciliis, M. A.; Di Furia, F.; Ballistreri, F. P.; Tomaselli, G. A. Toscano, R. M. The relative reactivity of thioethers and sulfoxides toward oxygen transfer reagents: The oxidation of thianthrene 5-oxide and related compounds by MoO5HMPT, *J. Org. Chem.* **1995**, *60,* 4475–4480.

[81] Kato, C. N.; Shinohara, A.; Hayashi, K.; Nomiya, K. Syntheses and X-ray Crystal Structures of Zirconium(IV) and Hafnium(IV) Complexes Containing Monovacant Wells–Dawson and Keggin Polyoxotungstates, *Inorg. Chem*. **2006**, *45*, 8108−8119.

[82] Sokolov, M.N.; Chubarova, E.V.; Peresypkina, E.V.; Virovets, A.V.; Fedin, V.P. Complexes of Zr^{IV} and Hf^{IV} with monolacunary Keggin and Dawson type anions. *Rus. Chem. Bull., Int. Ed.* **2007**, *56*, 220—224.

[83] Sokolov, M.N.; Izarova, N.V.; Peresypkina, E.V.; Mainichev, D.A.; Fedin, V.P. Zirconium and hafnium aqua complexes $[(H_2O)_3M(P_2W_{17}O_{61})]^{6-}$: synthesis, characterization and substitution of water by chiral ligand. *Inorg. Chim. Acta* **2009**, *362,* 3756–3762.

[84] Errington, R.J.; Petkar, S.S.; Middleton, P.S.; McFarlane, W.; Clegg, W.; Coxall, R.A.; Harrington, R.W. Synthesis and reactivity of the methoxozirconium pentatungstate $(^nBu_4N)_6[\{(\mu\text{-}MeO)ZrW_5O_{18}\}_2]$: insights into proton-transfer reactions, solution dynamics, and assembly of $\{ZrW_5O_{18}\}_2$-building blocks. *J. Am. Chem. Soc.* **2007**, *129*, 12181-12196.

[85] DFT calculations were performed with Gaussian16 using B3LYP functional. The basis set was lanl2dz for W, Ti, and Nb atoms and 6-31g(d,p) for the rest of the atoms. The solvent effects of acetonitrile were included using the IEF-PCM implicit solvation model. See the Supporting Information for details.

[86] Jiménez-Lozano, P.; Carbó, J.J.; Chaumont, A.; Poblet, J.M.; Rodríguez-Fortea, A.; Wipf, G. Nature of Zr-monosubstituted monomeric and dimeric polyoxometalates in water solution at different pH conditions: static density functional theory calculations and dynamic simulations. *Inorg. Chem.* **2014**, *53*, 778−786.

[87] Jiménez-Lozano, P.; Solé-Daura, A.; Wipf, G.; Poblet, J.M.; Chaumont, A.; Carbó, J.J. Assembly mechanism of Zr-containing and other TM-containing polyoxometalates. *Inorg. Chem*. **2017**, *56,* 4148-4156.

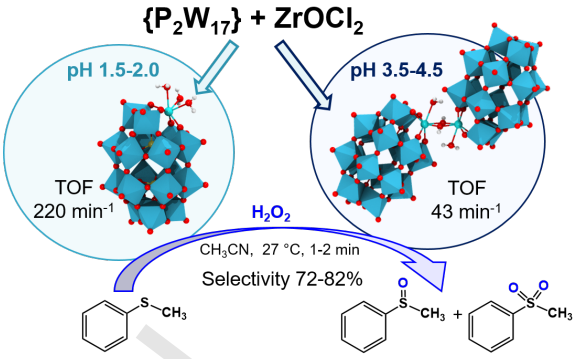
[88] Jiménez-Lozano, P.; Puiggalí-Jou, J..; Chaumont, A.; Carbó, J.J. Collective Behavior of Zr-Substituted Polyoxometalates in Solution: Insights from Molecular Dynamics Simulations. *Inorg. Chem.* **2025**, *64*, 8875−8884.

[89] Ivanchikova, I. D.; Maksimchuk, N. V.; Marikovskaya, S. M.; Evtushok, V. Yu.; Antonov, A. A.; Yanshole, V. V. Kholdeeva O. A. Activation of tert-butyl hydroperoxide by Zr(IV) stabilized by polyoxotungstate scaffolds. *ChemPlusChem* **2025**, *90*, e202400605.

Just Accepted

[90] Adam, W.; Haas, W.; Sieker, G. Thianthrene 5-oxide as mechanistic probe in oxygen transfer reactions: the case of carbonyl oxides vs. dioxiranes, *J. Amer. Chem. Soc.* **1984**, *106*, 5020–5022.
[91] Adam, W.; Golsch, D; Görth, F.C. Thianthrene 5-oxide as a mechanistic probe in oxygen transfer reactions: the case of carbonyl oxides versus dioxiranes revisited, *Chem. Eur. J.* **1996**, *2*, 255–258.
[92] Jiménez-Lozano, P.; Ivanchikova, I. D.; Kholdeeva, O. A.; Poblet, J. M.; Carbó, J. J. Alkene oxidation by Ti-containing polyoxometalates. Unambiguous characterization of the role of protonation state. Chem. Commun. **2012,** *48*, 9266–9268.
[93] Zalomaeva, O. V.; Maksimchuk, N. V.; Evtushok, V. Yu.; Antonov, A. A.; Yanshole, V. V.; Kholdeeva, O. A. Thioether oxidation with tert-butyl hydroperoxide catalyzed by Zr(IV)-substituted polyoxometalates. Mechanistic insights, *Dalton Transactions*, **2025**, 54, 12524 – 12533.
[94] Di Furia, F.; Modena, G. Mechanism of oxygen transfer from peroxo species, *Pure & Appl. Chem.* **1982**, *54*, 1853–1866.

© The Author(s) 20xx. *Polyoxometalates* published by Tsinghua University Press. The articles published in this open access journal are distributed under the terms of the Creative Commons Attribution 4.0 International License (http://creativecommons.org/licenses/by/4.0/), which permits use, distribution and reproduction in any medium, provided the original work is properly cited.



Acidity during the synthesis of a Zr-monosubstituted phosphotungstate of the Wells-Dawson structure strongly affects its composition/structure and catalytic activity in H_2O_2-based oxidation of thioethers

Just Accepted